good approximation for certain systems and that the qualitative behaviour of the motion can be understood by relatively simple analysis. In this context we will study systems that have applications to typical problems in the solar system, thereby excluding the more exotic variations of the three-body problem, such as the Copenhagen problem (where the two large masses are equal), the Pythagorean problem (where the three bodies have initial masses in the ratio 3:4:5 and initial positions on a 3,4,5 right-angled triangle), and triple collisions (where the three bodies can "pass through" one another).

In this chapter we describe the equations of motion of the three-body problem and discuss the location and stability of equilibrium points with particular reference to a constant of the motion, the Jacobi integral, in the circular restricted case. We demonstrate the relationship between curves defined by the Jacobi integral and the orbital path of the particle. We derive Hill's equations to study the motion of the particle in the vicinity of one of the masses and show the general properties of such a system. Finally, we discuss the effects of drag forces in the three-body problem.

3.2 Equations of Motion

We consider the motion of a small particle of negligible mass moving under the gravitational influence of two masses m_1 and m_2. We assume that the two masses have circular orbits about their common centre of mass and that they exert a force on the particle although the particle cannot affect the two masses.

Consider a set of axes ξ, η, ζ in the inertial frame referred to the centre of mass of the system (see Fig. 3.1). Let the ξ axis lie along the line from m_1 to m_2 at time $t = 0$ with the η axis perpendicular to it and in the orbital plane of the two masses and the ζ axis perpendicular to the ξ–η plane, along the angular momentum vector. Let the coordinates of the two masses in this reference frame be (ξ_1, η_1, ζ_1) and (ξ_2, η_2, ζ_2). The two masses have a constant separation and the same angular velocity about each other and their common centre of mass. Let the unit of mass be chosen such that $\mu = \mathcal{G}(m_1 + m_2) = 1$. If we now assume that $m_1 > m_2$ and define

$$\bar{\mu} = \frac{m_2}{m_1 + m_2} \tag{3.1}$$

then in this system of units the two masses are

$$\mu_1 = \mathcal{G}m_1 = 1 - \bar{\mu} \qquad \text{and} \qquad \mu_2 = \mathcal{G}m_2 = \bar{\mu}, \tag{3.2}$$

where $\bar{\mu} < 1/2$. The unit of length is chosen such that the constant separation of the two masses is unity. It then follows that the common mean motion, n, of the two masses is also unity.

Let the coordinates of the particle in the *inertial*, or *sidereal*, *system*, be (ξ, η, ζ). By applying the vector form of the inverse square law, the equations of

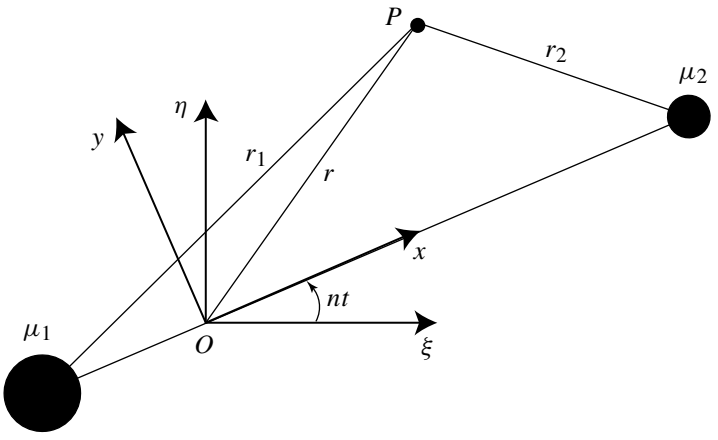

Fig. 3.1. A planar view of the relationship between the sidereal coordinates (ξ, η, ζ) and the synodic coordinates (x, y, z) of the particle at the point P. The origin O is located at the centre of mass of the two bodies. The ζ and z axes coincide with the axis of rotation and the arrow indicates the direction of positive rotation.

motion of the particle are

$$\ddot{\xi} = \mu_1 \frac{\xi_1 - \xi}{r_1^3} + \mu_2 \frac{\xi_2 - \xi}{r_2^3}, \tag{3.3}$$

$$\ddot{\eta} = \mu_1 \frac{\eta_1 - \eta}{r_1^3} + \mu_2 \frac{\eta_2 - \eta}{r_2^3}, \tag{3.4}$$

$$\ddot{\zeta} = \mu_1 \frac{\zeta_1 - \zeta}{r_1^3} + \mu_2 \frac{\zeta_2 - \zeta}{r_2^3}, \tag{3.5}$$

where, from Fig. 3.1,

$$r_1^2 = (\xi_1 - \xi)^2 + (\eta_1 - \eta)^2 + (\zeta_1 - \zeta)^2, \tag{3.6}$$

$$r_2^2 = (\xi_2 - \xi)^2 + (\eta_2 - \eta)^2 + (\zeta_1 - \zeta)^2. \tag{3.7}$$

Note that these equations are also valid in the general three-body problem since they do not require any assumptions about the paths of the two masses.

If the two masses are moving in circular orbits then the distance between them is fixed and they move about their common centre of mass at a fixed angular velocity, the mean motion n. In these circumstances it is natural to consider the motion of the particle in a rotating reference frame in which the locations of the two masses are also fixed. Consider a new, rotating coordinate system that has the same origin as the ξ, η system but which is rotating at a uniform rate n in the positive direction (see Fig. 3.1). The direction of the x axis is chosen such that the two masses always lie along it with coordinates $(x_1, y_1, z_1) = (-\mu_2, 0, 0)$ and

$(x_2, y_2, z_2) = (\mu_1, 0, 0)$. Hence, from Eq. (3.2) and Fig. 3.1 we have

$$r_1^2 = (x + \mu_2)^2 + y^2 + z^2, \tag{3.8}$$

$$r_2^2 = (x - \mu_1)^2 + y^2 + z^2, \tag{3.9}$$

where (x, y, z) are the coordinates of the particle with respect to the rotating, or *synodic*, *system*. These coordinates are related to the coordinates in the sidereal system by the simple rotation

$$\begin{pmatrix} \xi \\ \eta \\ \zeta \end{pmatrix} = \begin{pmatrix} \cos nt & -\sin nt & 0 \\ \sin nt & \cos nt & 0 \\ 0 & 0 & 1 \end{pmatrix} \begin{pmatrix} x \\ y \\ z \end{pmatrix}. \tag{3.10}$$

Although in our system of units $n = 1$, we will retain n in the equations to emphasise that all the terms in the equations of motion are accelerations.

If we now differentiate each component in Eq. (3.10) twice we obtain

$$\begin{pmatrix} \dot{\xi} \\ \dot{\eta} \\ \dot{\zeta} \end{pmatrix} = \begin{pmatrix} \cos nt & -\sin nt & 0 \\ \sin nt & \cos nt & 0 \\ 0 & 0 & 1 \end{pmatrix} \begin{pmatrix} \dot{x} - ny \\ \dot{y} + nx \\ \dot{z} \end{pmatrix} \tag{3.11}$$

and

$$\begin{pmatrix} \ddot{\xi} \\ \ddot{\eta} \\ \ddot{\zeta} \end{pmatrix} = \begin{pmatrix} \cos nt & -\sin nt & 0 \\ \sin nt & \cos nt & 0 \\ 0 & 0 & 1 \end{pmatrix} \begin{pmatrix} \ddot{x} - 2n\dot{y} - n^2 x \\ \ddot{y} + 2n\dot{x} - n^2 y \\ \ddot{z} \end{pmatrix}. \tag{3.12}$$

Note that the switch to a rotating reference frame has introduced terms in $n\dot{x}$ and $n\dot{y}$ (the *Corioli's acceleration*) and $n^2 x$ and $n^2 y$ (the *centrifugal acceleration*) into the equations of motion. Using these substitutions for ξ, η, ζ, $\ddot{\xi}$, $\ddot{\eta}$, and $\ddot{\zeta}$, Eqs. (3.3), (3.4), and (3.5) become

$$(\ddot{x} - 2n\dot{y} - n^2 x)\cos nt - (\ddot{y} + 2n\dot{x} - n^2 y)\sin nt = \left[\mu_1 \frac{x_1 - x}{r_1^3} + \mu_2 \frac{x_2 - x}{r_2^3}\right]\cos nt + \left[\frac{\mu_1}{r_1^3} + \frac{\mu_2}{r_2^3}\right] y \sin nt, \tag{3.13}$$

$$(\ddot{x} - 2n\dot{y} - n^2 x)\sin nt + (\ddot{y} + 2n\dot{x} - n^2 y)\cos nt = \left[\mu_1 \frac{x_1 - x}{r_1^3} + \mu_2 \frac{x_2 - x}{r_2^3}\right]\sin nt - \left[\frac{\mu_1}{r_1^3} + \frac{\mu_2}{r_2^3}\right] y \cos nt, \tag{3.14}$$

$$\ddot{z} = -\left[\frac{\mu_1}{r_1^3} + \frac{\mu_2}{r_2^3}\right] z. \tag{3.15}$$

If we multiply Eq. (3.13) by $\cos nt$, and Eq. (3.14) by $\sin nt$, and add the results, and then multiply Eq. (3.13) by $-\sin nt$, and Eq. (3.14) by $\cos nt$, and add these

together, the equations of motion in the synodic system become

$$\ddot{x} - 2n\dot{y} - n^2 x = -\left[\mu_1 \frac{x+\mu_2}{r_1^3} + \mu_2 \frac{x-\mu_1}{r_2^3}\right], \tag{3.16}$$

$$\ddot{y} + 2n\dot{x} - n^2 y = -\left[\frac{\mu_1}{r_1^3} + \frac{\mu_2}{r_2^3}\right] y, \tag{3.17}$$

$$\ddot{z} = -\left[\frac{\mu_1}{r_1^3} + \frac{\mu_2}{r_2^3}\right] z. \tag{3.18}$$

These accelerations can also be written as the gradient of a scalar function U:

$$\ddot{x} - 2n\dot{y} = \frac{\partial U}{\partial x}, \tag{3.19}$$

$$\ddot{y} + 2n\dot{x} = \frac{\partial U}{\partial y}, \tag{3.20}$$

$$\ddot{z} = \frac{\partial U}{\partial z}, \tag{3.21}$$

where $U = U(x, y, z)$ is given by

$$U = \frac{n^2}{2}(x^2 + y^2) + \frac{\mu_1}{r_1} + \frac{\mu_2}{r_2}. \tag{3.22}$$

In this equation the term in $x^2 + y^2$ is the centrifugal potential and the term in $1/r_2$ and $1/r_2$ is the gravitational potential, the partial derivatives of which give rise to the centrifugal and gravitational forces, respectively.

The $-2n\dot{y}$ and $+2n\dot{x}$ terms in Eqs. (3.19) and (3.20) are the Corioli's terms, which depend on the velocity of the particle in the rotating reference frame. The resulting Corioli's force is at right angles to the velocity and therefore does no work.

Note that in our definition U is positive. However, this is opposite to the practice in physics and is purely a convention in celestial mechanics. We could equally well have taken it to be negative, say $U^* = -U$, and the equations of motion would become

$$\ddot{x} - 2n\dot{y} = -\frac{\partial U^*}{\partial x}, \tag{3.23}$$

$$\ddot{y} + 2n\dot{x} = -\frac{\partial U^*}{\partial y}, \tag{3.24}$$

$$\ddot{z} = -\frac{\partial U^*}{\partial z}. \tag{3.25}$$

Note also that U is not a true potential and it is best referred to as a scalar function from which some (but not all) of the accelerations experienced by the particle in the rotating frame can be derived. U is called a "pseudo-potential."

3.3 The Jacobi Integral

Multiplying Eq. (3.19) by $\dot{x}$, and Eq. (3.20) by $\dot{y}$, and Eq. (3.21) by $\dot{z}$ and adding we have

$$\dot{x}\ddot{x} + \dot{y}\ddot{y} + \dot{z}\ddot{z} = \frac{\partial U}{\partial x}\dot{x} + \frac{\partial U}{\partial y}\dot{y} + \frac{\partial U}{\partial z}\dot{z} = \frac{\mathrm{d}U}{\mathrm{d}t}. \tag{3.26}$$

This can be integrated to give

$$\dot{x}^2 + \dot{y}^2 + \dot{z}^2 = 2U - C_\mathrm{J}, \tag{3.27}$$

where C_J is a constant of integration. Since $\dot{x}^2 + \dot{y}^2 + \dot{z}^2 = v^2$, the square of the velocity of the particle in the rotating frame, we have

$$v^2 = 2U - C_\mathrm{J} \tag{3.28}$$

or, using Eq. (3.22),

$$C_\mathrm{J} = n^2(x^2 + y^2) + 2\left(\frac{\mu_1}{r_1} + \frac{\mu_2}{r_2}\right) - \dot{x}^2 - \dot{y}^2 - \dot{z}^2. \tag{3.29}$$

This demonstrates that the quantity $2U - v^2 = C_\mathrm{J}$ is a constant of the motion. This is the *Jacobi integral*, or Jacobi constant, sometimes called the *integral of relative energy.* It is important to note that this is not an energy integral because in the restricted problem neither energy nor angular momentum is conserved. The Jacobi integral is the only integral of the circular restricted three-body problem and this means that the problem cannot be solved in closed form for general cases.

The expression for C_J can also be written in terms of the position and velocity of the particle in the nonrotating, sidereal frame. For the position vectors we can use Eq. (3.10) to obtain

$$\begin{pmatrix} x \\ y \\ z \end{pmatrix} = \begin{pmatrix} \cos nt & \sin nt & 0 \\ -\sin nt & \cos nt & 0 \\ 0 & 0 & 1 \end{pmatrix} \begin{pmatrix} \xi \\ \eta \\ \zeta \end{pmatrix}. \tag{3.30}$$

For the velocity vectors we can use Eq. (3.11) to obtain

$$\begin{pmatrix} \dot{x} - ny \\ \dot{y} + nx \\ \dot{z} \end{pmatrix} = \begin{pmatrix} \cos nt & \sin nt & 0 \\ -\sin nt & \cos nt & 0 \\ 0 & 0 & 1 \end{pmatrix} \begin{pmatrix} \dot{\xi} \\ \dot{\eta} \\ \dot{\zeta} \end{pmatrix}. \tag{3.31}$$

However,

$$\begin{pmatrix} \dot{x} - ny \\ \dot{y} + nx \\ \dot{z} \end{pmatrix} = \begin{pmatrix} \dot{x} \\ \dot{y} \\ \dot{z} \end{pmatrix} + n \begin{pmatrix} \sin nt & -\cos nt & 0 \\ \cos nt & \sin nt & 0 \\ 0 & 0 & 0 \end{pmatrix} \begin{pmatrix} \xi \\ \eta \\ \zeta \end{pmatrix} \tag{3.32}$$

and hence

$$\begin{pmatrix} \dot{x} \\ \dot{y} \\ \dot{z} \end{pmatrix} = \begin{pmatrix} \cos nt & \sin nt & 0 \\ -\sin nt & \cos nt & 0 \\ 0 & 0 & 1 \end{pmatrix} \begin{pmatrix} \dot{\xi} \\ \dot{\eta} \\ \dot{\zeta} \end{pmatrix} - n \begin{pmatrix} \sin nt & -\cos nt & 0 \\ \cos nt & \sin nt & 0 \\ 0 & 0 & 0 \end{pmatrix} \begin{pmatrix} \xi \\ \eta \\ \zeta \end{pmatrix}. \tag{3.33}$$

If we let

$$\mathbf{A} = \begin{pmatrix} \cos nt & \sin nt & 0 \\ -\sin nt & \cos nt & 0 \\ 0 & 0 & 1 \end{pmatrix} \quad \text{and} \quad \mathbf{B} = \begin{pmatrix} \sin nt & -\cos nt & 0 \\ \cos nt & \sin nt & 0 \\ 0 & 0 & 0 \end{pmatrix} \tag{3.34}$$

then, from Eq. (3.33),

$$\begin{aligned} \dot{x}^2 + \dot{y}^2 + \dot{z}^2 &= (\dot{x} \quad \dot{y} \quad \dot{z}) \begin{pmatrix} \dot{x} \\ \dot{y} \\ \dot{z} \end{pmatrix} \\ &= (\dot{\xi} \quad \dot{\eta} \quad \dot{\zeta})\, \mathbf{A}^{\mathrm{T}}\mathbf{A} \begin{pmatrix} \dot{\xi} \\ \dot{\eta} \\ \dot{\zeta} \end{pmatrix} - n\,(\dot{\xi} \quad \dot{\eta} \quad \dot{\zeta})\, \mathbf{A}^{\mathrm{T}}\mathbf{B} \begin{pmatrix} \xi \\ \eta \\ \zeta \end{pmatrix} \\ &\quad - n\,(\xi \quad \eta \quad \zeta)\, \mathbf{B}^{\mathrm{T}}\mathbf{A} \begin{pmatrix} \dot{\xi} \\ \dot{\eta} \\ \dot{\zeta} \end{pmatrix} + n^2\,(\xi \quad \eta \quad \zeta)\, \mathbf{B}^{\mathrm{T}}\mathbf{B} \begin{pmatrix} \xi \\ \eta \\ \zeta \end{pmatrix} \\ &= \dot{\xi}^2 + \dot{\eta}^2 + \dot{\zeta}^2 + n^2(\xi^2 + \eta^2) + 2n(\dot{\xi}\eta - \dot{\eta}\xi), \end{aligned} \tag{3.35}$$

where $\mathbf{A}^{\mathrm{T}}$ and $\mathbf{B}^{\mathrm{T}}$ denote the transposes of the matrices $\mathbf{A}$ and $\mathbf{B}$. Since $\mathbf{A}$ and $\mathbf{B}$ are both orthogonal matrices, their inverses are simply their transposes. Because distances are always unchanged by rotations (or, equivalently, since the determinants of orthogonal matrices are equal to unity) we also have $x^2+y^2+z^2 = \xi^2 + \eta^2 + \zeta^2$; this can also be obtained from Eq. (3.10). We obtain

$$C_{\mathrm{J}} = 2\left(\frac{\mu_1}{r_1} + \frac{\mu_2}{r_2}\right) + 2n(\xi\dot{\eta} - \eta\dot{\xi}) - \dot{\xi}^2 - \dot{\eta}^2 - \dot{\zeta}^2 \tag{3.36}$$

for the expression for the Jacobi constant in terms of the sidereal coordinates. We can rewrite this as

$$\frac{1}{2}\left(\dot{\xi}^2 + \dot{\eta}^2 + \dot{\zeta}^2\right) - \left(\frac{\mu_1}{r_1} + \frac{\mu_2}{r_2}\right) = \mathbf{h} \cdot \mathbf{n} - \frac{1}{2}C_{\mathrm{J}}, \tag{3.37}$$

where $\mathbf{n} = (0, 0, n)$ and the left-hand side of the equation is the total, or mechanical, energy per unit mass of the particle. Because $\mathbf{h} \cdot \mathbf{n}$ is not a constant, this explains why energy is not conserved in the restricted three-body problem.

The measurement of the particle's position and velocity in either frame determines the value of the Jacobi constant associated with the motion of the particle. The existence of the angular momentum and energy integrals in the two-body problem enabled us to solve for the motion of one mass with respect to the other (see Sect. 2.3). The Jacobi constant is the only integral of the motion in the

restricted three-body problem. We cannot make use of it to provide an exact solution for the orbital motion, but we can use it to determine regions from which the particle is excluded.

The usefulness of the Jacobi constant can be appreciated by considering the locations where the velocity of the particle is zero. In this case we have

$$2U = C_{\mathrm{J}} \tag{3.38}$$

or

$$n^2(x^2 + y^2) + 2\left(\frac{\mu_1}{r_1} + \frac{\mu_2}{r_2}\right) = C_{\mathrm{J}}. \tag{3.39}$$

Equation (3.39) defines a set of surfaces for particular values of C_{J}. These surfaces, known as the *zero-velocity surfaces*, play an important role in placing bounds on the motion of the particle. For simplicity we restrict ourselves to the x–y plane. In this case the intersection of the zero-velocity surfaces with the x–y plane produces a set of *zero-velocity curves*. Figure 3.2 shows examples of these curves for the case $\mu_2 = 0.2$; the mean motion n is taken to be unity. From our expression for the Jacobi constant, Eq. (3.27), it is clear that we must always have $2U \geq C_{\mathrm{J}}$ since otherwise the velocity v would be complex. Thus Eq. (3.39) defines the boundary curves of regions where particle motion is not possible, in other words excluded regions. Hence, although the restricted three-body problem is not integrable (we cannot solve for the motion of the particle for arbitrary starting conditions), the existence of the Jacobi integral does permit us to find regions of x–y space where the particle cannot be. The result is easily extended to three dimensions.

Since the shaded areas in Fig. 3.2 denote regions where motion is impossible, we can see from Fig. 3.2a, for example, that if a particle with that value of C_{J} is in orbit in the unshaded region around the mass μ_1 then it can never orbit the mass μ_2 or escape from the system since it would have to cross the excluded region to

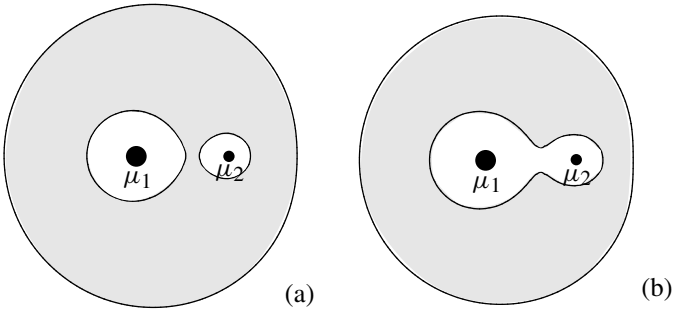

Fig. 3.2. Zero-velocity curves for two values of the Jacobi constant for the case when $\mu_2 = 0.2$. The values of C_{J} are (a) $C_{\mathrm{J}} = 3.9$, (b) $C_{\mathrm{J}} = 3.7$. The shaded areas denote the excluded regions. (See also Fig. 9.11 for the case $\mu_2 = 10^{-3}$.)

choice of starting conditions it is possible to find orbital solutions where the epicyclic motion is entirely suppressed and the particle's path is just the path of the epicentre.

3.9 Tadpole and Horseshoe Orbits

It is important to remember that the types of motion described by the solution of the equations for perturbed motion around L_4 and L_5 are only valid in the vicinity of these equilibrium points and, by implication, only for small amplitudes of libration. This means that we cannot deduce anything about the solution for large displacements from the equilibrium points. However, it is always possible to resort to numerical integration of the full equations of motion of the particle in the rotating frame; these were derived in Sect. 3.2 (see Eqs. (3.16) and (3.17)).

Figure 3.16 shows two separate trajectories obtained by integrating the full equations of motion for starting conditions in the vicinity of the L_4 point for $\mu_2 = 0.001$, a value similar to the Sun–Jupiter mass ratio. The trajectory shown in Fig. 3.16a has been started slightly closer to L_4 than the one shown in Fig. 3.16b. Note that in each case the path is more elongated ahead of the L_4 point. Furthermore, in Fig. 3.16a the orbit extends over 86°; the orbit that was started further from L_4 shown in Fig. 3.16b extends over 115°. Recalling that the two masses and L_4 form an equilateral triangle, the side of which is the unit of length, it is clear from Fig. 3.16 that both orbits move close to the unit circle centred on the mass μ_1 (cf. Fig. 3.9). The orbits shown in Fig. 3.16 are referred to as *tadpole orbits* because of the elongated shapes of the orbits (and the zero-velocity curves). The similarity is even more enhanced when orbits with zero free eccentricity are considered. Note that tadpole orbits also describe particle paths around the L_5 point.

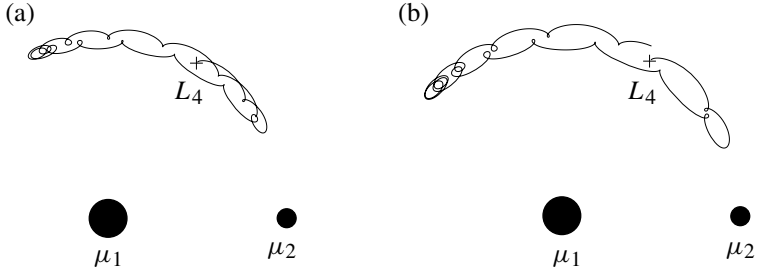

Fig. 3.16. Two examples of tadpole orbits librating about the L_4 equilibrium point (denoted by a cross and located at $x_0 = 1/2 - \mu_2$, $y_0 = \sqrt{3}/2$) for $\mu_2 = 0.001$. The masses μ_1 and μ_2 are denoted by the filled circles. (a) The starting conditions are $x = x_0 + 0.0065$, $y = y_0 + 0.0065$ with $\dot{x} = \dot{y} = 0$ and the orbit is followed for 15 orbital periods of μ_2. (b) The starting conditions are $x = x_0 + 0.008$, $y = y_0 + 0.008$ with $\dot{x} = \dot{y} = 0$ and the orbit is followed for 15.5 orbital periods of μ_2.

The question now arises as to what kind of orbit would we expect if we increase the initial radial separation from L_4 or L_5 even more? The answer is that provided the initial distance is not too large, the resulting orbit will encompass both L_4 and L_5. These are referred to as *horseshoe orbits* and two examples are shown in Fig. 3.17 using starting conditions taken from the paper by Taylor (1981). Note that the orbit shown in Fig. 3.17b has starting conditions that almost suppress the epicyclic motion, giving a smooth appearance to the path.

Comparison of the paths of the epicentres deduced from Figs. 3.16 and 3.17 with the form of the zero-velocity curves shown in Fig. 3.9 reveals striking similarities. However, it is important to note that the zero-velocity curves do not define the orbital paths, although, as we shall see in Sect. 3.10, there is a close connection between the two when μ_2 is small. Note that those orbits shown in Figs. 3.16 and 3.17 have zero initial velocities. Hence there is a zero-velocity curve associated with each of the orbits, although these have not been drawn. Such curves only guarantee that the orbits do not get too close to the L_4 and L_5 points and give no indication of the long-term stability of the orbits. However, remember that if the Jacobi constant of an orbit is less than that for L_4 and L_5, then a zero-velocity curve cannot be drawn and there are no excluded regions.

We can illustrate the properties of horseshoe and tadpole orbits for small mass ratios with a number of examples obtained from direct numerical integrations of the equations of motion. Figure 3.18 shows three trajectories (one horseshoe and two tadpole) for the case where $\mu_2 = 10^{-3}$. Here θ is the angle around the orbit, with $\theta = 0$ corresponding to the line from the primary mass to the secondary mass. All the orbits are started with eccentricity $e \approx 0$. Note that there is considerable variation of the semi-major axis around the orbit with the

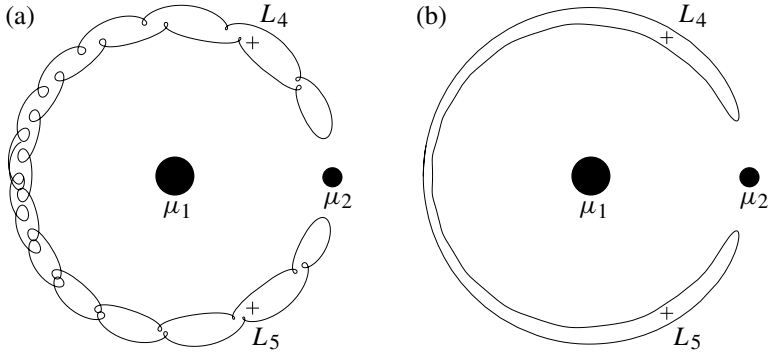

Fig. 3.17. Two examples of near-periodic horseshoe orbits librating about the L_4 equilibrium point for $\mu_2 = 0.000953875$, taken from data given by Taylor (1981). (a) The starting conditions are $x = -0.97668$, $y = \dot{x} = 0$, $\dot{y} = -0.06118$. (b) The starting conditions are $x = -1.02745$, $y = \dot{x} = 0$, $\dot{y} = 0.04032$.

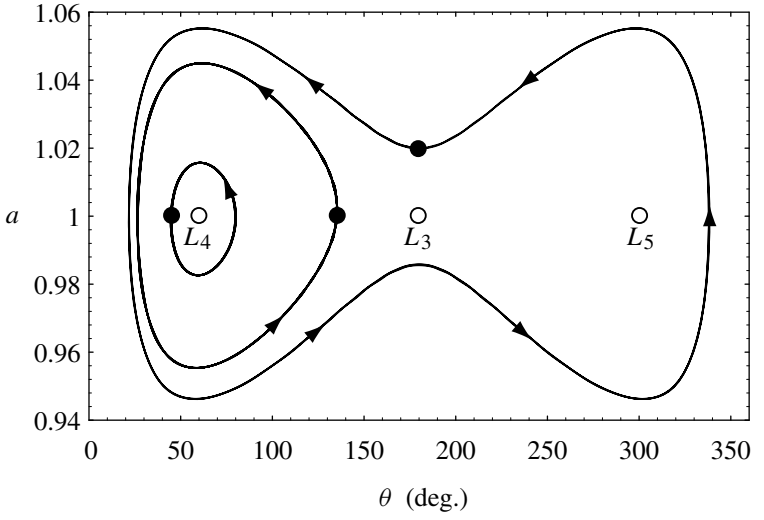

Fig. 3.18. The variation of semi-major axis a with the angle θ around the orbit for three trajectories with $\mu_2 = 10^{-3}$. The starting positions are indicated by filled circles and the enclosed equilibrium points with open circles. All orbits were followed for 100 orbital periods of the secondary mass and arrows indicate the direction of the motion.

maximum deviation from the unit circle occurring at the L_4 and L_5 equilibrium points. At these points the horseshoe and tadpoles have their maximum width. Note too that there is considerable asymmetry in the path. This is demonstrated by the fact that the L_3 point does not lie midway between the outer and inner branches of the horseshoe at $\theta = 180^\circ$. Although we are plotting the variation of a and not r around the path, there would be little difference because we have chosen $e \approx 0$. Therefore the loops apparent in Figs. 3.16 and 3.17 do not appear in this example.

The changes in a and e as a function of time for the horseshoe orbit (with $\mu_2 = 10^{-3}$) are shown in Fig. 3.19. The relatively sudden changes in a denote the effect of encounters with the secondary mass when the orbit switches from $a > 1$ to $a < 1$, or vice versa (see Fig. 3.19a). If we write $a = 1 + \Delta a$ and measure Δa every time $\theta = 180^\circ$ then an interesting phenomenon emerges. We chose an initial value of $\Delta a = 0.020$. After one encounter with the secondary $\Delta a = -0.0143$, but after two encounters measurements show that $\Delta a = 0.0198$, with the pattern repeating itself at subsequent encounters. This demonstrates that the asymmetry in $|\Delta a|$ is almost cancelled out after one complete cycle of the horseshoe. As we shall see in Sect. 3.15, this property can be useful in maintaining horseshoe orbits against the orbital decay produced by dissipation (Dermott et al. 1980, Dermott & Murray 1981a). It is clear from Fig. 3.19b that

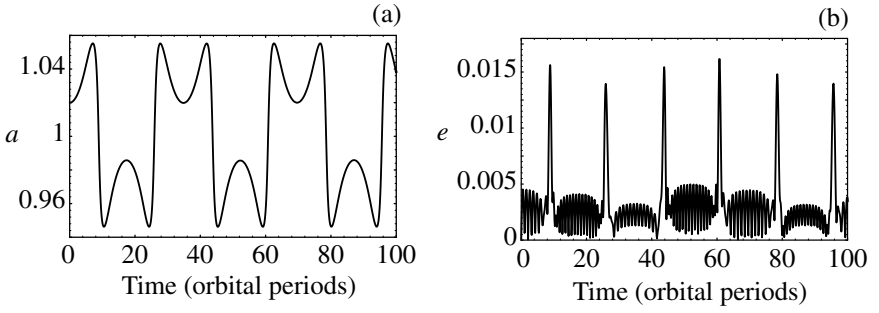

Fig. 3.19. The variation of (a) semi-major axis a, and (b) eccentricity e as a function of time for the horseshoe orbit shown in Fig. 3.18 for $\mu_2 = 10^{-3}$.

the encounters with the secondary also correspond to times of sudden changes in e, with an order of magnitude increase on approach and decrease on retreat. The small oscillations in eccentricity between encounters (which, in accordance with Tisserand's relation also have a maximum amplitude at the L_4 and L_5 points) imply that phase effects could be important. This helps to explain why there are variations in the magnitude of the eccentricity "impulse" at encounters, rather than the symmetry (after two encounters) shown in the variation in a.

The effect of a decrease in the mass ratio is shown in Figs. 3.20 and 3.21, where we show two of the equivalent plots for the case $\mu_2 = 10^{-6}$. Because of the decrease in μ_2 we have chosen the initial semi-major axis to be $a = 1.002$, (i.e., a value of Δa that is an order of magnitude smaller). The plot of the variation of a with θ shows, as before, that the paths have maximum width in a at $\theta = 60^\circ$ and $\theta = 300^\circ$, the locations of the L_4 and L_5 points. However, there are two subtle differences. Firstly, the degree of symmetry is more pronounced with L_3 now lying approximately midway between the values of a at $\theta = 180^\circ$. Secondly, although we have started both tadpoles with the same values of θ as before (135° and 45°) they have a smaller relative extent in a than their counterparts for $\mu_2 = 10^{-3}$. This implies that the radial extent of the tadpole zone with respect to the horseshoe zone has decreased with decreasing μ_2. For the tadpole orbit we have added its zero-velocity curve for comparison. Note that its radial width is always half that of the tadpole orbit, in keeping with our analytical result.

The extent of symmetry in the small-μ_2 case is clearly shown in Fig. 3.21. The integration shows that that while initially $\Delta a = 0.00200$, after one encounter $\Delta a = -0.00199$, and after two encounters $\Delta a = 0.00200$. If the long-term stability of a horseshoe orbit can be deduced from its proximity to a symmetric periodic orbit then this suggests that horseshoe orbits in the small-μ_2 case are highly stable. Examination of the changes in e shows that order of magnitude

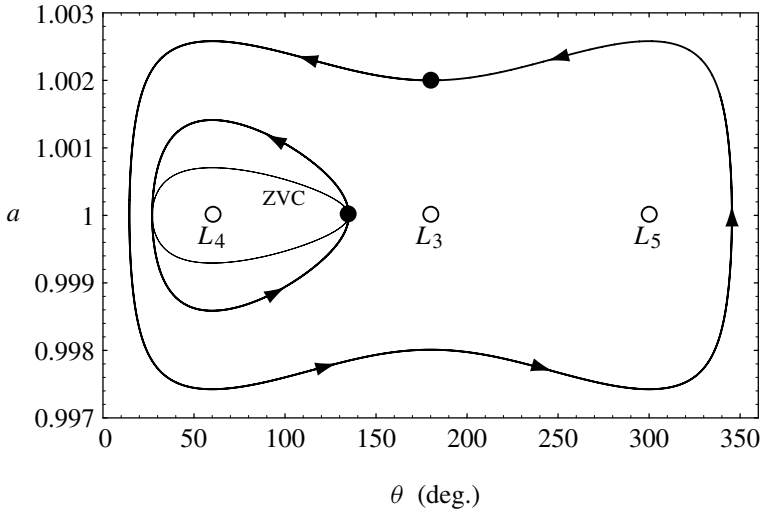

Fig. 3.20. The variation of semi-major axis a with the angle θ around the orbit for horseshoe and tadpole trajectories with $\mu_2 = 10^{-6}$. The starting positions are indicated by filled circles and the enclosed equilibrium points with open circles. The zero-velocity curve for the tadpole trajectory is the thin curve labelled ZVC. All orbits were followed for 1,000 orbital periods of the secondary mass and arrows indicate the direction of the motion.

changes still occur at encounters but the symmetry is much more pronounced than in the large μ_2 case.

If a starting condition is chosen that corresponds to a near-circular orbit either interior or exterior to the unit circle, then it is clear that the nature of the resulting orbit depends on the radial separation of the orbit from the unit circle. We have shown analytically and numerically how particles started close

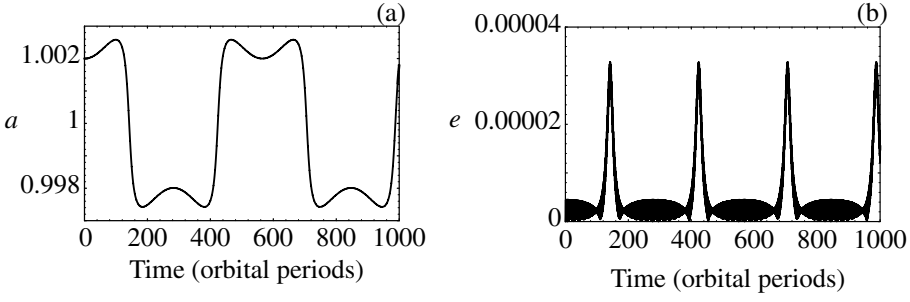

Fig. 3.21. The variation of (a) semi-major axis a, and (b) eccentricity e as a function of time for the horseshoe orbit shown in Fig. 3.20 for $\mu_2 = 10^{-6}$.

to L_4 and L_5 execute a small-amplitude libration about the equilibrium point. By increasing the initial separation the resulting orbit becomes more elongated in the direction of the L_3 point (tadpole orbits). Eventually particles started sufficiently far from the unit circle will librate about L_4, L_3, and L_5 (horseshoe orbits). However, particles moving sufficiently far from the unit circle will not give rise to orbits with a change in the direction of motion of the epicentre and the orbits are said to *circulate* interior or exterior to the unit circle. Depending on the value of the Jacobi constant it may be possible for the particle to encounter the mass μ_2.

3.10 Orbits and Zero-Velocity Curves

The zero-velocity curve that defines the limits of the forbidden region in Fig. 3.15 has an elongated shape and is tilted at an angle of $\sim 30^\circ$ to the horizontal. We can study the behaviour of such curves in the vicinity of the triangular equilibrium points by means of a translation of the origin, a rotation of 30°, and an expansion about the new origin. At the L_4 point, for example, we have $x = 1/2 - \mu_2$ and $y = \sqrt{3}/2$. The translation of the origin is achieved with the substitutions $x \to (1/2 - \mu_2) + x$ and $y \to \sqrt{3}/2 + y$ in Eqs. (3.8) and (3.9). A rotation of the coordinate system by 30° about the new origin is achieved by a substitution $x \to \sqrt{3}x'/2 + y'/2$ and $y \to -x'/2 + \sqrt{3}y'/2$, where x' and y' are the new values of x and y. This gives

$$r_1^2 = 1 + 2y' + x'^2 + y'^2, \tag{3.154}$$

$$r_2^2 = 1 - \sqrt{3}x' + y' + x'^2 + y'^2. \tag{3.155}$$

From Eq. (3.22) the transformed equation defining the zero-velocity curves, $C_\mathrm{J} = 2U$, is given by

$$C_\mathrm{J} = 1 - \mu_2 - \sqrt{3}\mu_2 x' + (2 - \mu_2)y' + x'^2 + y'^2 + 2\left(\frac{(1-\mu_2)}{r_1} + \frac{\mu_2}{r_2}\right), \tag{3.156}$$

where terms of $\mathcal{O}(\mu_2^2)$ have been neglected. Expanding Eq. (3.156) about the new origin we obtain

$$C_\mathrm{J} \approx 3 - \mu_2 + \frac{9}{4}\mu_2 x'^2 + 3y'^2. \tag{3.157}$$

In this expansion we have neglected terms of order three and higher as well as terms involving $\mu_2 y'$ since (i) μ_2 is assumed to be a small quantity and (ii) the shapes of the zero-velocity curves shown in Fig. 3.9 suggest that the radial extent of the curves is small for small μ_2; note that the term in $\mu_2 x$ vanishes without making any approximation. In effect our approximation amounts to neglecting the curvature of the resulting curves along the unit radius. If we write

$$C_\mathrm{J} = 3 + \gamma\mu_2, \tag{3.158}$$